

# Nanoscale Atoms in Solid-State Chemistry

Xavier Roy,<sup>1</sup> Chul-Ho Lee,<sup>1,2</sup> Andrew C. Crowther,<sup>3</sup> Christine L. Schenck,<sup>1</sup> Tiglet Besara,<sup>4</sup> Roger A. Lalancette,<sup>6</sup> Theo Siegrist,<sup>4,5</sup> Peter W. Stephens,<sup>7</sup> Louis E. Brus,<sup>1</sup> Philip Kim,<sup>2</sup> Michael L. Steigerwald,<sup>1\*</sup> Colin Nuckolls<sup>1\*</sup>

<sup>1</sup>Department of Chemistry, Columbia University, New York, NY 10027, USA. <sup>2</sup>Department of Physics, Columbia University, New York, NY 10027, USA. <sup>3</sup>Department of Chemistry, Barnard College, New York, NY 10027, USA. <sup>4</sup>National High Magnetic Field Laboratory, FSU, Tallahassee, FL 32310, USA. <sup>5</sup>Department of Chemical and Biomedical Engineering, FAMU-FSU College of Engineering, Tallahassee, FL 32310, USA. <sup>6</sup>Department of Chemistry, Rutgers State University, Newark, NJ 07102, USA. <sup>7</sup>Department of Physics and Astronomy, SUNY Stony Brook, Stony Brook, NY 11794, USA.

\*Corresponding author. E-mail: cn37@columbia.edu (C.N.); mls2064@columbia.edu (M.L.S.)

**We describe a solid-state material formed from binary assembly of atomically precise molecular clusters.  $[\text{Co}_6\text{Se}_8(\text{PET}_3)_6][\text{C}_{60}]_2$  and  $[\text{Cr}_6\text{Te}_8(\text{PET}_3)_6][\text{C}_{60}]_2$  assembled into a superatomic relative of the  $\text{CdI}_2$  structure type. These solid-state materials showed activated electronic transport with activation energies of 100 to 150 millielectron volts. The more reducing cluster  $\text{Ni}_9\text{Te}_6(\text{PET}_3)_8$  transferred more charge to the fullerene and formed a rock-salt related structure. In this material, the constituent clusters are able to interact electronically to produce a magnetically ordered phase at low temperature, akin to atoms in a solid-state compound.**

Conventional binary solid-state compounds,  $\text{A}_x\text{B}_y$ , are infinite, crystalline arrays of atoms A and B. Here we describe analogous binary solids in which the “atomic” building blocks are pseudo-spherical molecular clusters rather than simply atoms [for reviews on molecular clusters, see (1–3)]. We prepare these new solids by simply combining independently synthesized molecular clusters (4–6). The internal structures of the constituent clusters remain unchanged, but charge is transferred between them, forming ionic solids analogous to NaCl. We report three new solids:  $[\text{Co}_6\text{Se}_8(\text{PET}_3)_6][\text{C}_{60}]_2$ ,  $[\text{Cr}_6\text{Te}_8(\text{PET}_3)_6][\text{C}_{60}]_2$ , and  $[\text{Ni}_9\text{Te}_6(\text{PET}_3)_8][\text{C}_{60}]$ . The former two assemble into a superatomic relative of the  $\text{CdI}_2$  structure type, and the latter forms a simple rock-salt crystal.

Despite their ready availability, molecular clusters have been used infrequently as electronic materials. Noteworthy examples of success in this area are the organic-inorganic hybrid materials reported by Batail and Mitzi (7–11). Nanocrystals have been assembled into striking superlattices (12–14), but they do not have discrete structural, electronic and magnetic properties and cannot be regarded as genuine artificial atoms. Here, we combine independently prepared electronically and structurally complementary molecular cluster building blocks to form atomically precise binary solid-state compounds. When the building blocks are atoms (ions), binary solids assemble into simple crystalline arrays such as the rock-salt and  $\text{CdI}_2$  lattices [for an authoritative text on solid-state inorganic chemistry, see (15)]. We show that when similarly-sized clusters combine the same lattice results, albeit at the dramatically increased length scale of nanometers rather than Angstroms. The constituent clusters interact to produce collective properties such as electrically conducting networks and magnetic ordering.

Our strategy was to use constituent molecular clusters that have the same, roughly spherical, shape but very different electronic properties in order to encourage reaction and subsequent structural association. By analogy to “atomic” solid-state chemistry, we reasoned that the in situ transfer of charge would produce ions (or the equivalent) that could then form an ordered solid. Thus, we sought cluster pairs in which one cluster

is relatively electron-poor and the other is relatively electron-rich.  $\text{C}_{60}$  carbon clusters are good electron acceptors (16). The electrically neutral metal chalcogenide clusters  $\text{Co}_6\text{Se}_8(\text{PET}_3)_6$  (**1**),  $\text{Cr}_6\text{Te}_8(\text{PET}_3)_6$  (**2**), and  $\text{Ni}_9\text{Te}_6(\text{PET}_3)_8$  (**3**) are all electron-rich. Importantly, these clusters (Fig. 1) are similar in size and shape to the fullerene.

We combined **1** and two equivalents of  $\text{C}_{60}$  in toluene and obtained black crystals after ~12 hours. Single-crystal x-ray diffraction (SCXRD) revealed that this solid is a 1:2 stoichiometric combination of **1** and  $\text{C}_{60}$  (**1**· $2\text{C}_{60}$ ) (Fig. 2, A and B) composed of hexagonal arrays of  $\text{C}_{60}$ s in a chair-like arrangement separated by layers of the clusters. The  $\text{C}_{60}$  layers are 12.5 Å apart. The centroid-to-centroid distance and the shortest non-bonded C-C spacing between two adjacent  $\text{C}_{60}$ 's are 9.9 Å and 3.4 Å, respectively. These distances are comparable to crystalline  $\text{C}_{60}$  (17). We obtain the exact same structure when we combine the  $\text{Cr}_6\text{Te}_8(\text{PET}_3)_6$  cluster **2** and two

equivalents of  $\text{C}_{60}$  in toluene (figs. S2 and S3) (18).

We measured how much charge was transferred between the components in the solid-state material using Raman spectroscopy. The  $A_{2g}$  pentagonal pinch mode of  $\text{C}_{60}$  (1468  $\text{cm}^{-1}$  for pristine  $\text{C}_{60}$ ) shifts to lower energy by 6  $\text{cm}^{-1}$  per electron transferred to  $\text{C}_{60}$  independent of the dopant or the crystal structure [see, for example, (19); for a review on discrete fullerene anions, see (20)]. The solid-state Raman spectra of **1**· $2\text{C}_{60}$  and **2**· $2\text{C}_{60}$  (fig. S4) (18) were taken using a 514.5 nm excitation laser at 4.6–7.8  $\text{kW}/\text{cm}^2$  power densities. The  $A_{2g}$  modes of  $\text{C}_{60}$  were centered at 1463  $\text{cm}^{-1}$  and 1462  $\text{cm}^{-1}$  in **1**· $2\text{C}_{60}$  and **2**· $2\text{C}_{60}$ , respectively. The difference between the  $A_{2g}$  peak position of **1**· $2\text{C}_{60}$  and **2**· $2\text{C}_{60}$  is small and within experimental error. We estimate that clusters **1** and **2** transfer two electrons, and each  $\text{C}_{60}$  receives one electron.

The solid-state electronic absorption spectra of **1**· $2\text{C}_{60}$  and **2**· $2\text{C}_{60}$  provide additional confirmation for the formation of charge transfer complexes in the materials. The electronic spectra of both materials dispersed in KBr pellets show a series of transitions between 900 and 1150 nm with the strongest band centered at 1100 nm (figs. S6 and S7) (18). These features are transitions for the radical anion of fullerene,  $\text{C}_{60}^{\cdot-}$  (20). Cluster **1** has four weak transitions between 350 and 700 nm that were observed in **1**· $2\text{C}_{60}$  but not in **2**· $2\text{C}_{60}$ .

We can compare these solids to traditional simple  $\text{M}^{2+}\text{X}^{1-}_2$  solids. The  $\text{CdI}_2$  structure type (21) is formed by a hexagonally close-packed array of monoanions with half of the octahedral interstitial sites occupied by dications. The cations are ordered such that along the crystallographic *c*-direction the cation layers are alternatively empty and fully occupied, and the layers are held together by van der Waals bonding between anions of neighboring layers. The structures of compounds **1**· $2\text{C}_{60}$  and **2**· $2\text{C}_{60}$  can be appreciated in these same terms. Wireframe representation of **1**· $2\text{C}_{60}$  are shown in Fig. 3; in Fig. 3A we compare one  $\text{C}_{60}$ -cluster- $\text{C}_{60}$  layer to the corresponding layer in  $\text{CdI}_2$ . In panels (B), (C) and (D) we show edge-on and packing views of these same layers; the similarity between our cluster-solid and the “atomic” solid is evident. Although atomic solid  $\text{CdI}_2$  appears in many different polytypes, which are related

by different patterns of stacking of *ab* planes, we have observed only one stacking polytype in our cluster solids.

The cluster  $\text{Ni}_9\text{Te}_6(\text{PEt}_3)_8$  (**3**) is rich in metal, and we expect this compound to have a greater reducing power than **1** or **2**. Interdiffusion of cluster **3** and  $\text{C}_{60}$  solutions for two weeks at  $-30^\circ\text{C}$  gives a black solid that is composed of micron-sized cubic crystals. Rietveld refinement of the synchrotron powder x-ray diffraction data (fig. S1) (18) reveals a 1:1 combination of **3** and  $\text{C}_{60}$  ( $3\cdot\text{C}_{60}$ ) (Fig. 2C) in a face-centered cubic structure analogous to rock salt with a lattice parameter of 21.7 Å. We observed a broad peak centered at  $1454\text{ cm}^{-1}$  in the solid-state Raman spectrum of  $3\cdot\text{C}_{60}$  (fig. S5) (18). We assign this peak to the  $A_{2g}$  mode of  $\text{C}_{60}$ , and these data strongly suggest that the fullerene in  $3\cdot\text{C}_{60}$  is more reduced than in  $1\cdot 2\text{C}_{60}$  or  $2\cdot 2\text{C}_{60}$ . These results show that we can prepare binary cluster materials with diverse structural and ionic properties by changing the composition of the molecular cluster building block.

These materials behave less like molecular co-crystals and more like three-dimensional solid-state compounds. For example,  $1\cdot 2\text{C}_{60}$  and  $2\cdot 2\text{C}_{60}$  exhibit activated electronic transport. Figure 4A displays the electrical transport properties of the co-crystals  $1\cdot 2\text{C}_{60}$  (fig. S9 shows the transport properties of  $2\cdot 2\text{C}_{60}$ ) (18) We performed two and four probe measurements on single crystals and pressed pellets of  $1\cdot 2\text{C}_{60}$  and two probe measurements on pressed pellets of  $2\cdot 2\text{C}_{60}$ . Both compounds are good electrical conductors with resistivities on the order of 10 ohm-cm at room temperature. We observe an exponential decrease of the conductance (*G*) with decreasing temperature. This thermally activated semiconducting behavior displayed Arrhenius behavior with activation energies  $E_a$  of  $\sim 150\text{ meV}$  and  $\sim 100\text{ meV}$  for  $1\cdot 2\text{C}_{60}$  and  $2\cdot 2\text{C}_{60}$ , respectively, and indicates that  $1\cdot 2\text{C}_{60}$  and  $2\cdot 2\text{C}_{60}$  are both gapped semiconductors.

An additional feature of these superatom-assembled solids is that the magnetic properties vary as the inorganic cores are changed because of the vastly different spin states accessible with the molecular clusters. Figure 4B shows the temperature dependence of the inverse molar magnetic susceptibility ( $1/\chi_M$ ) and the effective magnetic moment ( $\mu_{\text{eff}}$ ) of  $1\cdot 2\text{C}_{60}$  from SQUID magnetometry. We corrected the data for diamagnetic and temperature-independent contributions and modeled the results using a modified Curie-Weiss law

$$\chi_M(T) = \frac{C}{T - \Theta} + \chi_D + \chi_{TIP}$$

where *C* is the Curie constant,  $\Theta$  is the Weiss constant, and  $\chi_D$  and  $\chi_{TIP}$  are the diamagnetic and temperature independent paramagnetic contributions, respectively. A good fit is obtained with  $C = 0.9\text{ emu K Oe}^{-1}\text{ mol f.u.}^{-1}$  (f.u. = formula unit),  $\Theta = -0.3\text{ K}$  and  $\chi_{TIP} = 0.001\text{ emu Oe}^{-1}\text{ mol f.u.}^{-1}$ . The small negative Weiss constant indicates weak antiferromagnetic interactions. Above 10 K,  $1\cdot 2\text{C}_{60}$  showed a temperature-independent effective magnetic moment,  $\mu_{\text{eff}} = 2.7\ \mu_B$  per f.u. This result agreed well with the spin-only value of  $2.8\ \mu_B$  for two non-interacting unpaired electrons and is consistent with the Raman spectroscopy data that show one electron in each of the two  $\text{C}_{60}$ s per formula unit, with the cobalt ions in the cluster not contributing to the overall moment.

Figure 4B also displays the temperature dependence of the inverse molar magnetic susceptibility ( $1/\chi_M$ ) of  $2\cdot 2\text{C}_{60}$ . The important result is that  $2\cdot 2\text{C}_{60}$  exhibits a more complex magnetic behavior with a change in the slope of this plot around 60 K. We presume the difference in the materials is caused by the large magnetic difference between compound (**1**)<sup>2+</sup>, which contains six  $\text{Co}^{\text{III}}$ , and compound (**2**)<sup>2+</sup>, which is composed of six  $\text{Cr}^{\text{III}}$ .

The magnetism of the rock-salt  $3\cdot\text{C}_{60}$  material is remarkably different from that of  $1\cdot 2\text{C}_{60}$  and  $2\cdot 2\text{C}_{60}$  both in magnitude and as a function of temperature. Figure 4C shows the temperature dependence of the magnetization (*M*) of  $3\cdot\text{C}_{60}$ . When we applied a field of 200 Oe and

cooled the sample to 2 K, we measured no appreciable magnetic response until the temperature reached about 4 K, at which point we observed a sudden transition to a magnetically ordered phase with *M* reaching  $2300\text{ emu mol f.u.}^{-1}$  at 2 K. The difference between the zero-field cooled (ZFC) and field-cooled (FC) magnetizations indicates some irreversibility in the magnetically ordered phase. The magnetic response of  $3\cdot\text{C}_{60}$  to an external field differs dramatically when the sample is examined at temperatures above  $T_c$  and below  $T_c$  (Fig. 4D). At  $T = 10\text{ K}$ , *M* scales linearly with *H*. The sigmoidal magnetization curve measured at 2 K is characteristic of ferromagnetism. Compound  $1\cdot\text{C}_{60}$  exhibits a small hysteresis with a coercivity  $H_c \sim 400\text{ Oe}$ . This indicates that the spins freeze in a ferromagnetic state for  $T < T_c$ . This result demonstrates that the constituent clusters are able to communicate magnetically at low temperature in the same way that atoms are able to in solid-state compounds.

By using clusters that are similar in size and shape to each other, we have created binary assemblies whose infinite crystalline structures are determined not only by the shapes of the clusters but also by the degree of charge transfer between the constituents. The intercluster charge transfer, along with the intermolecular van der Waals interactions that are typical in conventional molecular solids, hold these solid-state compounds together in much the same way that interatomic charge transfer from Cd to I holds  $\text{CdI}_2$  together and from Na to Cl holds rock-salt together. These results chart a clear path to creating whole families of multifunctional solid-state materials whose electronic and magnetic properties can be tuned by varying the constitution of the superatom building blocks.

## References and Notes

- S. A. Claridge *et al.*, Cluster-assembled materials. *ACS Nano* **3**, 244 (2009). doi:10.1021/nn800820e Medline
- D. L. Long, E. Burkholder, L. Cronin, Polyoxometalate clusters, nanostructures and materials: From self assembly to designer materials and devices. *Chem. Soc. Rev.* **36**, 105 (2007). doi:10.1039/b502666k Medline
- M. W. Degroot, J. F. Corrigan, in *Comprehensive Coordination Chemistry II*, J. A. McCleverty, T. J. Meyer, Eds. (Pergamon, Oxford, 2003), pp. 57–123.
- X. Roy *et al.*, Quantum soldering of individual quantum dots. *Angew. Chem. Int. Ed.* **51**, 12473 (2012). doi:10.1002/anie.201206301 Medline
- B. Hesse, T. Siegrist, T. Palstra, S. M. Tazler, M. L. Steigerwald, Hexakis(triethylphosphine)octatelluridohexachromium and a molecule-based synthesis of  $\text{Cr}_3\text{Te}_4$ . *Inorg. Chem.* **32**, 5165 (1993). doi:10.1021/ic00075a037
- J. G. Brennan, T. Siegrist, S. M. Stuczynski, M. L. Steigerwald, The transitions from molecules to solids: Molecular syntheses of  $\text{Ni}_9\text{Te}_6(\text{PEt}_3)_8$ ,  $\text{Ni}_{26}\text{Te}_{18}(\text{PEt}_3)_{12}$  and  $\text{NiTe}$ . *J. Am. Chem. Soc.* **111**, 9240 (1989). doi:10.1021/ja00208a023
- S. A. Baudron *et al.*, (EDT-TTF-CONH2)<sub>6</sub>[Re6Se8(CN)<sub>6</sub>], a metallic Kagome-type organic-inorganic hybrid compound: Electronic instability, molecular motion, and charge localization. *J. Am. Chem. Soc.* **127**, 11785 (2005). doi:10.1021/ja0523385 Medline
- D. B. Mitzi, Synthesis, structure, and properties of organic-inorganic perovskites and related materials. *Prog. Inorg. Chem.* **48**, 1 (1999). doi:10.1002/9780470166499.ch1
- A. Penicaud, P. Batail, C. Coulon, E. Canadell, C. Perrin, Novel redox properties of the paramagnetic hexanuclear niobium cluster halide  $\text{Nb}_6\text{Cl}_{18}^{3-}$  and the preparation, structures, and conducting and magnetic properties of its one-dimensional mixed-valence tetramethyltetra(selenium and thia)fulvalenium salts: [TMTSF and TMTTF]<sub>5</sub>[ $\text{Nb}_6\text{Cl}_{18}$ ]( $\text{CH}_2\text{Cl}_2$ )<sub>0.5</sub>. *Chem. Mater.* **2**, 123 (1990). doi:10.1021/cm00008a011
- P. Batail *et al.*, Antiperovskite structure with ternary tetrathiafulvalenium salts: Construction, distortion, and antiferromagnetic ordering. *Angew. Chem. Int. Ed. Engl.* **30**, 1498 (1991). doi:10.1002/anie.199114981
- C. Coulon, C. Livage, L. Gonzalez, K. Boubekeur, P. Batail, Electronic magnetic resonance in a series of antiferromagnetic molecular perovskites. *J. Phys. C*, **13**, 1153 (1993). doi:10.1051/jp1:1993262
- E. Auyeung *et al.*, Synthetically programmable nanoparticle superlattices using a hollow three-dimensional spacer approach. *Nat. Nanotechnol.* **7**, 24

- (2012). [doi:10.1038/nnano.2011.222](https://doi.org/10.1038/nnano.2011.222) [Medline](#)
13. A. G. Dong, J. Chen, P. M. Vora, J. M. Kikkawa, C. B. Murray, Binary nanocrystal superlattice membranes self-assembled at the liquid-air interface. *Nature* **466**, 474 (2010). [doi:10.1038/nature09188](https://doi.org/10.1038/nature09188) [Medline](#)
  14. M. V. Kovalenko, M. Scheele, D. V. Talapin, Colloidal nanocrystals with molecular metal chalcogenide surface ligands. *Science* **324**, 1417 (2009). [doi:10.1126/science.1170524](https://doi.org/10.1126/science.1170524) [Medline](#)
  15. A. F. Wells, *Structural Inorganic Chemistry* (Oxford Univ. Press, Oxford, ed. 5, 1984).
  16. Q. S. Xie, E. Perezcordero, L. Echegoyen, Electrochemical detection of  $C_{60}^{6-}$  and  $C_{70}^{6-}$ : Enhanced stability of fullerides in solution. *J. Am. Chem. Soc.* **114**, 3978 (1992). [doi:10.1021/ja00036a056](https://doi.org/10.1021/ja00036a056)
  17. W. I. F. David *et al.*, Crystal-structure and bonding of ordered  $C_{60}$ . *Nature* **353**, 147 (1991). [doi:10.1038/353147a0](https://doi.org/10.1038/353147a0)
  18. Materials and methods are available as supplementary materials on *Science* Online.
  19. H. Kuzmany, M. Matus, B. Burger, J. Winter, Raman-scattering in  $C_{60}$  fullerenes and fullerides. *Adv. Mater.* **6**, 731 (1994). [doi:10.1002/adma.19940061004](https://doi.org/10.1002/adma.19940061004)
  20. C. A. Reed, R. D. Bolskar, Discrete fulleride anions and fullerenium cations. *Chem. Rev.* **100**, 1075 (2000). [doi:10.1021/cr980017o](https://doi.org/10.1021/cr980017o) [Medline](#)
  21. R. M. Bozorth, The crystal structure of cadmium iodide. *J. Am. Chem. Soc.* **44**, 2232 (1922). [doi:10.1021/ja01431a019](https://doi.org/10.1021/ja01431a019)
  22. P. W. Betteridge, J. R. Carruthers, R. I. Cooper, K. Prout, D. J. Watkin, CRYSTALS version 12: Software for guided crystal structure analysis. *J. Appl. Cryst.* **36**, 1487 (2003). [doi:10.1107/S0021889803021800](https://doi.org/10.1107/S0021889803021800)
  23. E. J. Gabe, Y. Lepage, J. P. Charland, F. L. Lee, P. S. White, NRCVAX: An interactive program system for structure-analysis. *J. Appl. Cryst.* **22**, 384 (1989). [doi:10.1107/S0021889889003201](https://doi.org/10.1107/S0021889889003201)
  24. A. A. Coelho, TOPAS Academic, available at [www.topas-academic.net](http://www.topas-academic.net).
  25. A. M. Rao *et al.*, Photoinduced polymerization of solid  $C_{60}$  films. *Science* **259**, 955 (1993). [doi:10.1126/science.259.5097.955](https://doi.org/10.1126/science.259.5097.955)

**Acknowledgments:** This work was supported primarily through the Center for Re-Defining Photovoltaic Efficiency Through Molecular-Scale Control, an Energy Frontier Research Center (EFRC) funded by the U.S. Department of Energy (DOE), Office of Science, Office of Basic Energy Sciences under award DE-SC0001085. X.R. thanks the Natural Sciences and Engineering Research Council of Canada for a postdoctoral fellowship. C.-H.L. is partially supported by the Basic Science Research Program through the National Research Foundation of Korea (357-2011-1-C00035). C.L.S. is supported by the National Science Foundation Graduate Research Fellowship under award DGE-1144155. We thank Ysutomo Uemura for the SQUID magnetometer. NHMFL was supported in part by the National Science Foundation Cooperative Agreement DMR-1157490, the State of Florida, the U.S. Department of Energy, and Florida State University. Use of the National Synchrotron Light Source, Brookhaven National Laboratory, was supported by the U.S. Department of Energy, Office of Basic Energy Sciences under Contract DE-AC02-98CH10886. Structural analysis work done by T.B. and T.S. is supported by the U.S. Department of Energy, Office of Basic Sciences under Contract DE-SC0008832, the State of Florida, and Florida State University. The crystallographic data presented in this work are available through the Cambridge Crystallographic Data Center referencing deposition numbers: 940469-940472.

#### Supplementary Materials

[www.sciencemag.org/cgi/content/full/science.1236259/DC1](http://www.sciencemag.org/cgi/content/full/science.1236259/DC1)

Materials and Methods

Figs. S1 to S9

Table S1

References (22–25)

7 February 2013; accepted 21 May 2013

Published online 6 June 2013

10.1126/science.1236259

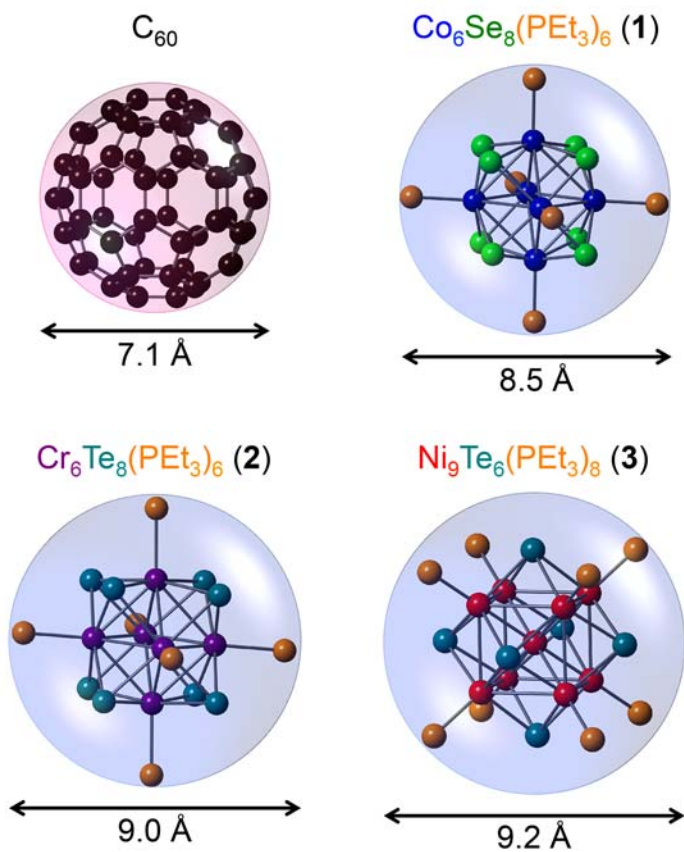


**Fig. 1.** Structures of the  $C_{60}$ ,  $Co_6Se_8(PEt_3)_6$ ,  $Cr_6Te_8(PEt_3)_6$ , and  $Ni_9Te_6(PEt_3)_8$  molecular building blocks as measured by single crystal x-ray diffraction. In the figure, the clusters are depicted on the same size scale. The diameter of the cluster is determined as the long diagonal P-P distance. The ethyl groups on the phosphines of **1**, **2** and **3** were removed to clarify the view.

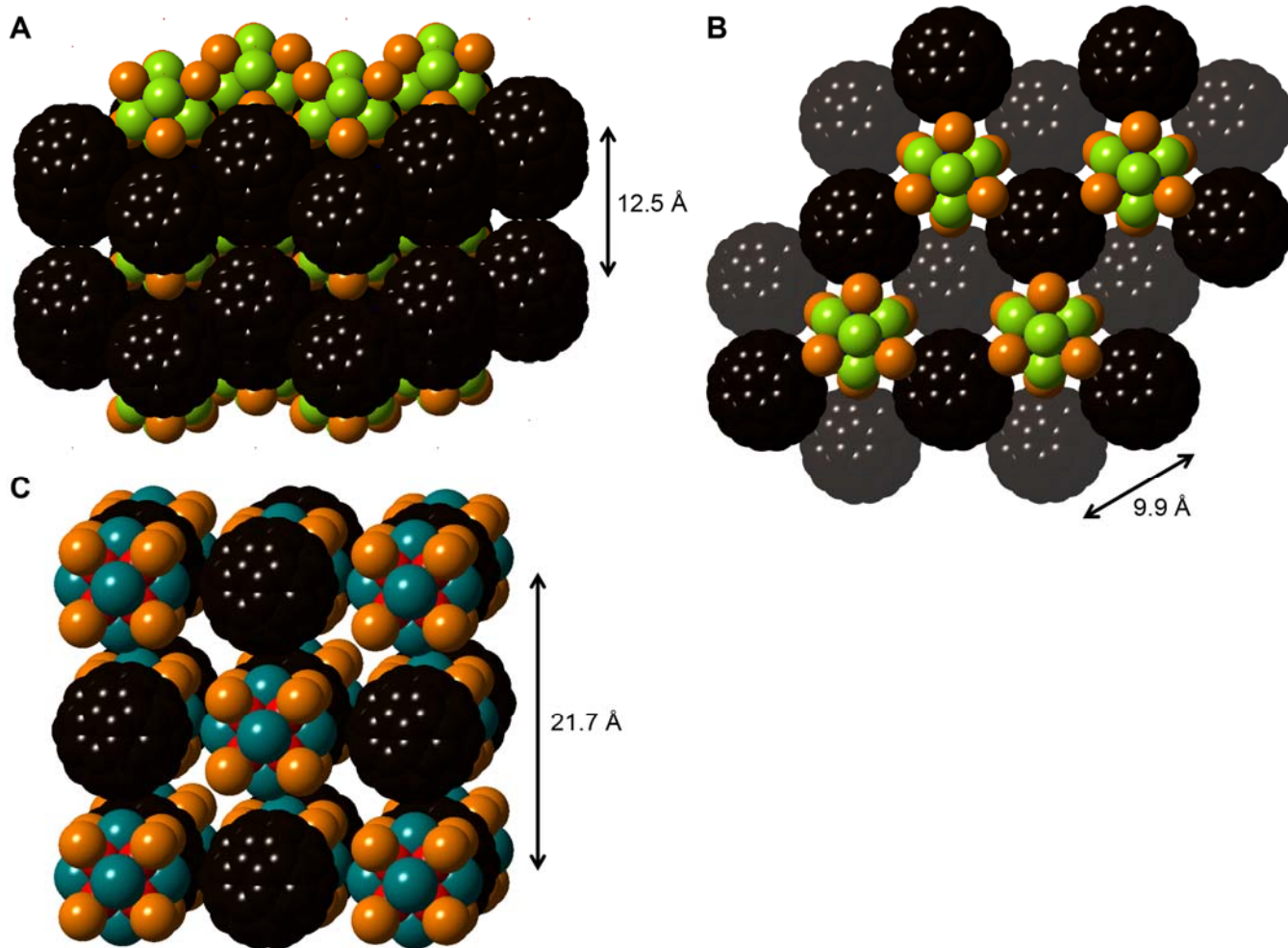


**Fig. 2.** Space filling molecular structure of  $1 \cdot 2C_{60}$  showing the crystal packing looking down (A) the  $ab$  plane and (B) the  $c$ -axis. (C) Space filling molecular structure of  $3 \cdot C_{60}$ . Carbon, black; nickel, red; cobalt, blue; phosphorus, orange; tellurium, teal; selenium, green. The ethyl groups on the phosphines were removed to clarify the view.

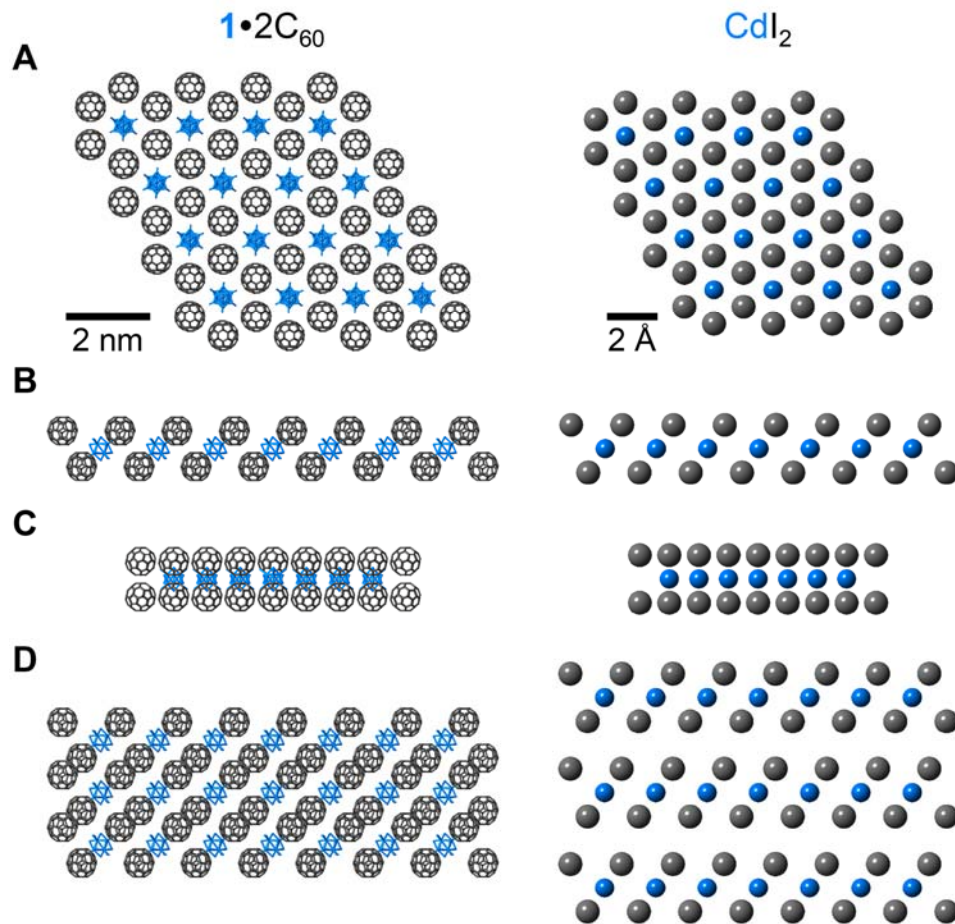


**Fig. 3.** Comparison of the packing structures of  $1 \cdot 2C_{60}$  and  $CdI_2$ . (A) View of a single hexagonal layer looking down the  $c$ -axis. (B) and (C) Edge-on views of the same layer looking down the  $ab$ -plane. (D) Stacking of the  $ab$  hexagonal layers along the  $c$ -axis direction. Cluster 1 and Cd are shown in blue;  $C_{60}$  and I are shown in grey. The ethyl groups on the phosphines were removed to clarify the view.

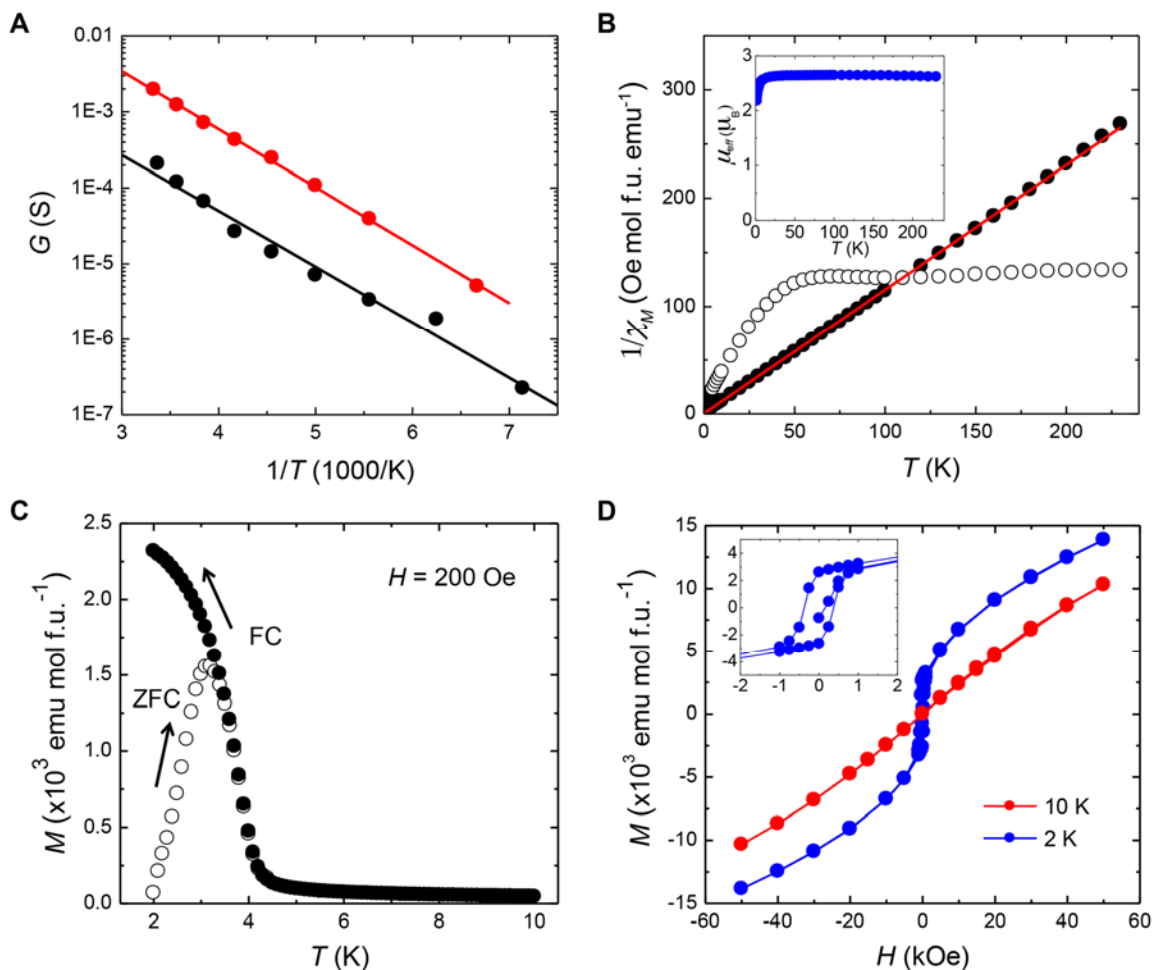


**Fig. 4.** (A) Plot of the conductance versus  $1/T$  for  $1\bullet 2C_{60}$ . The four probes conductance measurements were done on a single crystal (black) and a pressed pellet (red). The Arrhenius fits are shown as solid lines. (B) Inverse magnetic susceptibility (black) as a function of temperature for  $1\bullet 2C_{60}$  (circles) and  $2\bullet 2C_{60}$  (open circles) in an applied external field  $H = 1$  T. The Curie-Weiss fit for  $1\bullet 2C_{60}$  is shown in red. The effective magnetic moment of  $1\bullet 2C_{60}$  as a function of temperature is shown in the inset. (C) Temperature dependence of the ZFC and FC magnetization ( $M$ ) of  $3\bullet C_{60}$  in an applied external field  $H = 200$  Oe. In the ZFC experiment, the sample was cooled from room temperature to 2 K in zero-field prior to the measurement of  $M$  from 2 K to 10 K. (D) Magnetization as a function of applied field at 10 K and 2 K for  $3\bullet C_{60}$ . The inset shows the enlarged magnetic hysteresis at 2 K.